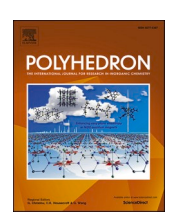


Contents lists available at ScienceDirect

Polyhedron

journal homepage: www.elsevier.com/locate/poly





Exploring different equatorial donors in a series of five-coordinate Cu(II) complexes supported by rigid tetradentate ligands

Anthony Devdass ^{a, 1}, Kallol Talukdar ^{a, 1}, Matthias Zeller ^b, Ryan C. Fortenberry ^a, Jonah W. Jurss ^{a, *}

ARTICLE INFO

Keywords:
Preorganized tetradentate ligands
Trigonal bipyramidal
Square pyramidal
Copper
Redox chemistry
Reorganization Energy

ABSTRACT

A series of tetradentate mixed-donor ligands has been synthesized containing an amine, thioether, or phosphine donor at the 8-position of a 2-(1,1-di(pyridin-2-yl)ethyl)quinoline backbone. Upon metalation with $CuCl_2$, the preorganized N_4 , N_3P , and N_3S donor ligands enforce distorted trigonal bipyramidal coordination environments around the copper metal center, in which a chlorido donor occupies the remaining axial coordination site. The complexes were characterized by elemental analysis, high-resolution mass spectrometry, and X-ray crystallography. The non-pyridyl equatorial donor was the sole difference from among the tetradentate ligands, and is responsible for the structural and electronic variations across the series. Indeed, more intermediate geometries between the ideal trigonal bipyramidal and square pyramidal extremes are observed with the larger phosphorus and sulfur donors. Relative to the N_4 derivative, the N_3P and N_3S systems have greater chemical stability upon redox cycling as observed in spectroelectrochemical experiments and lower inner-sphere reorganization energies for the $Cu^{II/I}$ redox couples based on density functional theory calculations.

1. Introduction

Copper complexes exist in a variety of geometries depending on their coordination number and ligand environment. $\mathrm{Cu^{II}}$ (d⁹) complexes often exhibit coordination numbers of 4 (square planar or tetrahedral), 5 (square pyramidal or trigonal bipyramidal), or 6 (octahedral or tetragonal) due to having a half-filled $\mathrm{d_z}^2$ orbital where the ligand field stabilization energy (LFSE) can help to rationalize the adopted geometry [1]. Intermediate and distorted geometries of $\mathrm{Cu^{II}}$ complexes are frequently observed as dictated by the electronic and steric properties of the ligand(s) [2]. On the other hand, $\mathrm{Cu^{I}}$ (d¹⁰) complexes are generally found to have coordination numbers of 2 (linear), 3 (trigonal planar), or 4 (tetrahedral), and have no particular preference that can be attributed to LFSE [3].

In nature, copper-containing metalloproteins exist in Cu^{II} and Cu^{II} oxidation states with varying geometries. The Cu sites in these enzymes are known to facilitate important reactions, such as electron transfer (i.e. plastocyanin), O_2 binding and transport (i.e. hemocyanin), substrate oxidation (i.e. galactose oxidase) and reduction (i.e. nitrite reductase),

and substrate activation (i.e. quercetinase) [3]. Copper proteins have traditionally been classified into three groups based on their spectroscopic properties [4]. Type I copper (T1Cu), or blue copper proteins, have been extensively studied and are characterized by a strong absorption band near 600 nm that gives rise to their blue color [5]. This group characteristically has one copper atom bound to two histidine imidazole nitrogens and one cysteine thiolate sulfur in a trigonal planar geometry. Based on the number and type of axial ligands, Type I copper proteins are further divided into three classes [6]. Class I T1Cu has one weakly bound methionine thioether donor in an axial position resulting in a distorted tetrahedral geometry as in plastocyanin [7]. Class II T1Cu has a non-methionine axial ligand with a distorted tetrahedral geometry as in umecyanin [8], while Class III T1Cu enzymes have two axial ligands, one being methionine and the other a glycine carbonyl oxygen donor, resulting in a distorted trigonal bipyramidal geometry as with azurin [9]. Type II (T2Cu) copper proteins are colorless and have fewer geometric restrictions relative to T1Cu copper enzymes. The most common ligand in this group is histidine as found in Cu,Zn superoxide dismutase (Cu,Zn SOD) [10]. Type III (T3Cu) copper proteins are

^a Department of Chemistry and Biochemistry, University of Mississippi, University, MS 38677, USA

^b Department of Chemistry, Purdue University, West Lafayette, IN 47907, USA

^{*} Corresponding author.

E-mail address: jwjurss@olemiss.edu (J.W. Jurss).

 $^{^{1}\,}$ A.D. and K.T. contributed equally.

binuclear in nature and are characterized by a strong absorption band near 300 nm. Each T3Cu center is bound to three histidine nitrogens in a trigonal planar geometry and when bound to dioxygen, the geometry transforms to square pyramidal with a bridging μ -peroxo between two copper centers as observed with hemocyanin [11,12]. The surrounding environment of copper protein active sites also influences the metal redox properties which is a critical component of substrate specificity [13]. Finally, a new group of copper enzymes was reported by Gray and co-workers in the last decade called Type zero (T0Cu) copper proteins, first found in T2 C112D variant of *Pseudomonas aeruginosa* azurin [14]. This group has a four-coordinate structure and adopts a pseudote-trahedral geometry around the copper site with two histidine donors, monodentate ligation from the carbonyl group of aspartate, and an axial carbonyl donor from glycine [15,16].

Several Cu^{II} model complexes have been synthesized to obtain insight into the nature of copper protein active sites [17-19]. Most of these model complexes involve ligand substitution and/or functionalization as an effort to match the spectroscopic and redox properties of the desired metalloproteins [20,21]. One appealing modification has been to use unsaturated nitrogen or sulfur donors as surrogates for the Ndonor histidine or S-donor cysteine and methionine residues that are present in copper enzymes [22,23]. A growing interest has emerged in using thioether donors due to their presence in copper enzymes and their ability to promote more anodic redox potentials of the copper center. Redox and spectroscopic properties of copper complexes supported by tetradentate N₃S, N₂S₂, and NS₃ donor ligands have been investigated as model complexes [24-26]. Most of these ligands are tripodal and have considerable flexibility to accommodate the metal center. Likewise, Kaim and co-workers reported 8-alkylthioquinoline and 8-arylthioquinoline-based copper complexes and studied the effects of steric constraints on the reversibility of the Cu^{II/I} redox couple [27]. It was shown that 8-alkylthioquinoline imine-S/thioether-S based chelate ligands were able to stabilize both the Cu^{II} and Cu^I oxidation states by adjusting the stereochemistry to minimize structural reorganization during the redox event. Such an adjustment was possible due to a certain degree of rotation by S atoms along the N-Cu-N axis [27].

Against this backdrop, we report a series of copper complexes supported by mixed-donor ligands containing an amine, thioether, or phosphine donor at the 8 position of a quinoline-based polypyridyl backbone (Scheme 1). The quinoline-based fragment features two pyridine donors at the 2 position *via* an sp³ carbon bridgehead to give a common core within the tetradentate mixed-donor ligands. We sought to explore the effects of donor substitution on the redox and spectroscopic properties of the copper complexes and reasoned that the rigidity

of the ligands would impose a constrained geometry around the metal center. Indeed, in the solid-state, the preorganized $N_4,\,N_3P,$ and N_3S donor ligands enforce distorted trigonal bipyramidal coordination environments around copper, in which a chlorido donor occupies the remaining axial coordination site. In contrast, the copper complexes reported by Kaim and co-workers have square pyramidal geometries supported by N_2S_2 donor environments [27]. The structures and properties of the complexes reported herein are discussed in the context of other five-coordinate Cu^{II} model complexes.

2. Results and discussion

2.1. Synthesis of the ligands and the complexes

The new family of tetradentate mixed-donor ligands was prepared in gram scale *via* a modular synthetic route with good to excellent yields (Scheme 1). Starting material 1,1-bis(2-pyridyl)ethane (1) was prepared from 2-ethylpyridine and 2-fluoropyridine following a published procedure [28]. A three-step synthesis from 2-bromoaniline afforded the central quinoline intermediate, 2,8-dibromoquinoline (2) [29]. The difference in reactivity of the bromine atoms of 2 allowed a selective nucleophilic aromatic substitution of the bromine at the 2-position using an organolithium intermediate prepared by treating 1 with *n*-butyllithium. The resulting common intermediate 3 was then subjected to palladium-catalyzed Buchwald-Hartwig cross coupling reactions with aniline, diphenylphosphine, and thiophenol to install the equatorial N, P, and S donors, respectively. The final ligands were isolated by column chromatography as off-white to light-yellow solids, and characterized by ¹H and ¹³C NMR and high-resolution mass spectrometry (Figs. S1-S13).

Metalation was achieved by stirring a 1:1 mixture of copper(II) chloride and the respective ligand in methanol under inert atmosphere. The complexes were purified by crystallization from concentrated solutions of acetonitrile or acetone by slow diffusion of diethyl ether at reduced temperature. The complexes are air and moisture stable in the solid state. The purity and composition of the complexes were confirmed by elemental analysis.

2.2. X-ray crystallography

The molecular structures of the three new complexes featuring N_4 , N_3P , and N_3S donor ligands were analyzed by single crystal X-ray diffraction. The data collection parameters and related unit cell information are listed in Table S1 of the Supporting Information. We note that X-ray quality crystals were not obtained for $[Cu(N_4)Cl](PF_6)$ or $[Cu(N_4)Cl](PF_6)$

Scheme 1. Synthesis of the N₄, N₃P, and N₃S donor ligands and their corresponding metal complexes.

Fig. 1. Crystal structures of $[Cu(N_4)Cl]$ Cl (left), $[Cu(N_3P)Cl]$ (PF₆) (middle), and $[Cu(N_3S)Cl]$ (PF₆) (right) with thermal ellipsoids rendered at the 70% probability level. Hydrogen atoms, except for the H atom on N4 in $[Cu(N_4)Cl]$ Cl, and outer-sphere counter ions and solvent molecules have been omitted for clarity.

 (N_3S) Cl]Cl; however, suitable crystals were grown and subsequently analyzed for the $[Cu(N_4)Cl]$ Cl and $[Cu(N_3S)Cl](PF_6)$ salts, respectively. Thermal ellipsoid plots of the cations are presented in Fig. 1 and selected bond distances and angles are provided in Table 1.

The rigid preorganized nature of the ligands affects the molecular structures of the complexes in several ways compared to reported Cu^{II} complexes. Here, the Cu^{II} center in each case features a five-coordinate geometry in a [(N₃L)Cl] coordination environment; each ligand binds in a tetradentate fashion with an anionic chlorido ligand at the fifth coordination site. The four donor atoms of each ligand form 5-membered chelate rings with the metal center. Distorted trigonal bipyramidal geometries are enforced by the ligands, in which the quinoline (N_q) and chlorido ligands occupy the axial sites, and the two pyridines (N_{py}) and the amine, phosphine, or thioether donor (L_{eq}) bind in the equatorial positions.

 Cu^{II} complexes supported by tetradentate ligands often prefer five-coordinate geometries [30–35]. Extensive structural and physicochemical studies of such complexes, including Cu^{II} model complexes, have revealed a continuum of structures between the ideal square pyramidal (SP) and trigonal bipyramidal (TBP) geometries [30–35]. In order to quantify the distortion from the ideal SP and TBP extremes, a geometric index τ was introduced by Addison et al. [18]. Using equation (1), τ values were calculated to determine the relative amount of trigonality in the five-coordinate systems where an ideal SP geometry has $\tau=0$, and for an ideal TBP geometry, $\tau=1$.

$$\tau = (\beta - \alpha)/60\tag{1}$$

In equation (1), β and α are defined as the largest and second largest L-M-L angles, respectively, in the structure.

The calculated τ values for $[Cu(N_4)Cl]^+$, $[Cu(N_3P)Cl]^+$, and $[Cu(N_3S)Cl]^+$ are 0.673, 0.561, and 0.543, respectively. These values indicate that the complexes have distorted trigonal bipyramidal geometries with the degree of distortion being greater for $[Cu(N_3P)Cl]^+$ and $[Cu(N_3S)Cl]^+$ relative to $[Cu(N_4)Cl]^+$. Given the single donor

 $\label{eq:complexes} \begin{tabular}{ll} \textbf{Table 1} \\ \textbf{Selected bond distances and angles of the } [Cu(N_3L)Cl]^+ \ complexes. \end{tabular}$

Bond distances and angles	[Cu(N ₄)C	1] +	[Cu(N ₃ P)Cl] +	[Cu(N ₃ S)Cl] ⁺
Cu-N _{pv1}	2.083(5)	2.111(5)	2.044(2)	2.075(2)
Cu-N _{pv2}	2.117(4)	2.087(4)	2.074(2)	2.076(2)
Cu-L _{eq}	2.099(5)	2.105(5)	2.2452(7)	2.3340(7)
Cu-N _q	1.973(4)	1.972(5)	2.049(2)	2.004(2)
Cu-Cl	2.227(1)	2.224(1)	2.2730(7)	2.2434(6)
Cu_{disp}	0.209	0.206	0.165	0.131
N _{pv1} -Cu-N _{pv2}	88.0(2)	88.6(2)	90.36(8)	87.55(8)
N _{pv1} -Cu-L _{eq}	132.3(2)	131.1(2)	141.65(6)	130.54(6)
N _{py2} -Cu-L _{eq}	135.7(2)	136.8(2)	125.96(6)	140.68(6)
N _{py1} -Cu- N _q	85.9(2)	84.7(2)	87.34(7)	88.07(8)
N _{py2} -Cu- N _q	83.9(2)	85.8(2)	84.69(7)	86.86(8)
L _{eq} -Cu-N _q	82.1(2)	82.2(2)	84.64(5)	85.36(6)
N _q -Cu-Cl	176.1(1)	177.4(1)	175.32(5)	173.24(6)
C ₁₇ -C ₂₁ -L _{eq}	116.4(5)	116.7(4)	114.6(1)	118.1(2)
τ	0.673	0.676	0.561	0.543

[a] Bond distances are in angstroms (Å) and bond angles are in degrees (°).

substitution across the series, this increase in distortion appears to stem from the larger third-row donor atom in the equatorial planes of the N_3S and N_3P complexes relative to the amine N-donor of $[Cu(N_4)Cl]^+$.

The equatorial pyridines are linked by an sp³ carbon bridgehead and the Cu-N_{py} bond distances range from 2.044 to 2.117 Å within the series, which is comparable to reported copper polypyridyl TBP complexes (Tables S1 and S2). Significantly different Cu-L_{eq} bond distances are observed for the varied equatorial donors. The much shorter Cu–N bond distance (0.146 and 0.235 Å shorter than the Cu-P and Cu-S bonds, respectively) is expected on the basis of atomic size. However, in comparing the Cu-P and Cu-S bond distances, the strong π accepting nature of the phosphine donor results in a noticeably shorter bond. Additional evidence of metal–ligand backbonding with the phosphine is apparent in the smaller $\rm C_{17}\text{-}C_{21}\text{-}L_{eq}$ angle of $[\text{Cu(N}_3\text{P)Cl]}^+$ relative to the same angle in $[\text{Cu(N}_3\text{S)Cl]}^+$.

The Cu-S bond length of $[Cu(N_3S)Cl]^+$ is 2.3340(7) Å, which is comparable to reported S-bound five-coordinate Cu^{II} complexes (Table S4) [21,24,27,35]. However, the Cu-N and Cu-P bond distances of $[Cu(N_4)Cl]^+$ and $[Cu(N_3P)Cl]^+$ are somewhat shorter than comparable bond lengths measured in related complexes (Tables S3 and S5). We note that phosphorus donors in five-coordinate Cu^{II} complexes, and thus closely related Cu-P bond distances, are rare in the literature.

The angle formed by the nitrogen donors of the dipyridyl arm and the metal center in each complex is approximately 90° . As a consequence of this acute angle, the remaining equatorial angles are greater than the 120° value expected for an ideal TBP geometry. In $[Cu(N_4)Cl]^+$, the difference between the two larger equatorial angles is 3.5° . However, in $[Cu(N_3P)Cl]^+$ and $[Cu(N_3S)Cl]^+$, the difference is 15.69 and 10.14° , respectively. The small difference in these angles for $[Cu(N_4)Cl]^+$ may be due to the presence of an outersphere chloride ion or water molecule in the crystal lattice that is engaged in hydrogen bonding with the secondary amine (Fig. S14).

The central quinoline donor (Nq) and chloride donor occupy axial sites of the [Cu(N₃L)Cl]⁺ complexes. The N_q-Cu-Cl axes deviate slightly (3.9 to 6.8°) from linearity with the degree of distortion tracking with the calculated $\boldsymbol{\tau}$ values. The Cu-N_{q} and Cu-Cl bond distances are consistent with related five-coordinate CuII complexes (Tables S2 and S6). However, $[Cu(N_4)Cl]^+$ exhibits the shortest axial bond distances within the series. The axial bond distances are slightly longer in [Cu $(N_3P)Cl$ + compared to the other two complexes, which is presumably due to the steric bulk exerted by the diphenylphosphine fragment. The amine and thioether donors at this position bear a single phenyl substituent. The effect of the single-site donor substitution (Lea) is also apparent by the displacement of the Cu^{II} ions from the planes defined by the three equatorial donors of each complex. The Cu^{II} ion resides above the plane, toward the chloride donor, at displacement distances (Cudisp) of 0.206, 0.165, and 0.131 Å from the equatorial plane of $[Cu(N_4)Cl]^{-1}$ $[Cu(N_3P)Cl]^+$, and $[Cu(N_3S)Cl]^+$, respectively. In this respect, the coordination pocket formed by the N_3S ligand is the most suitable for the Cu^{II} ion within the series.

2.3. UV-visible spectroscopy

The UV-visible spectrum of each complex was recorded in anhydrous acetonitrile (CH3CN) as seen in Fig. 2, and molar extinction coefficients (ε) were accurately determined by serial dilution (Figs. S15-17). As stated earlier, five-coordinate copper complexes are known to exist in geometries on a continuum between square pyramidal and trigonal bipyramidal [30–33]. In previous studies, the structures of fivecoordinate copper complexes in solution have been qualitatively determined by examining their absorption spectra [32]. We also note that molecular structures determined from solid-state measurements may not always reflect the molecular structure in solution [36,37]. Several polyamine Cu^{II} complexes with SP geometries are known to have metal-centered absorption bands (or d-d transitions) between 580 and 670 nm [38-40], while those with TBP geometry have d-d transitions between 780 and 950 nm [32,41-44]. Related Cu^{II} complexes with intermediate geometries in solution have absorption bands appearing in between these ranges [21,33]. In some cases, the prominent (or more intense) band appears with a lower intensity shoulder, which can be either higher or lower in energy than the prominent band. A higher energy band with a weak shoulder on the lower energy side indicates a geometry that favors SP, while a lower energy peak featuring a weak high energy shoulder indicates a more TBP geometry [36,37].

In this context, two absorption bands are seen in the visible and nearinfrared region of the spectra for all three complexes. [Cu(N₄)Cl] + has a higher intensity band at 656 nm ($\varepsilon = 248 \text{ M}^{-1}\text{cm}^{-1}$) and a lower energy shoulder at 752 nm ($\varepsilon = 220 \text{ M}^{-1}\text{cm}^{-1}$). A similar pattern is observed for $[Cu(N_3S)Cl]^+$ with the higher intensity band at 649 nm (ε = 324 M⁻¹cm⁻¹) and a lower energy shoulder at 739 nm (ε = 305 M⁻¹cm⁻¹). However, the intensity of these bands are much closer to one another than those of the N₄ complex. [Cu(N₃P)Cl] + has two broad bands of equal intensity at 577 ($\epsilon = 460~\text{M}^{-1}\text{cm}^{-1}$) and 655 nm ($\epsilon = 460~\text{M}^{-1}$ $M^{-1}cm^{-1}$). The transitions for $[Cu(N_3P)Cl]^+$ are consistent with its calculated τ value, which shows an intermediate geometry and considerable distortion from an ideal TBP geometry as shown by similar pentacoordinated Cu^{II} complexes [36,45-47]. The nature of the dd transitions in $[Cu(N_4)Cl]^+$ and $[Cu(N_3S)Cl]^+$ (to a lesser extent) indicate that these complexes favor distorted square pyramidal geometries in solution, consistent with observations by Algarra et al. of a 5-coordinate Cu(II) complex supported by a tris(2-aminoethyl)amine-based ligand [32]. Additional absorption bands of moderate intensity are

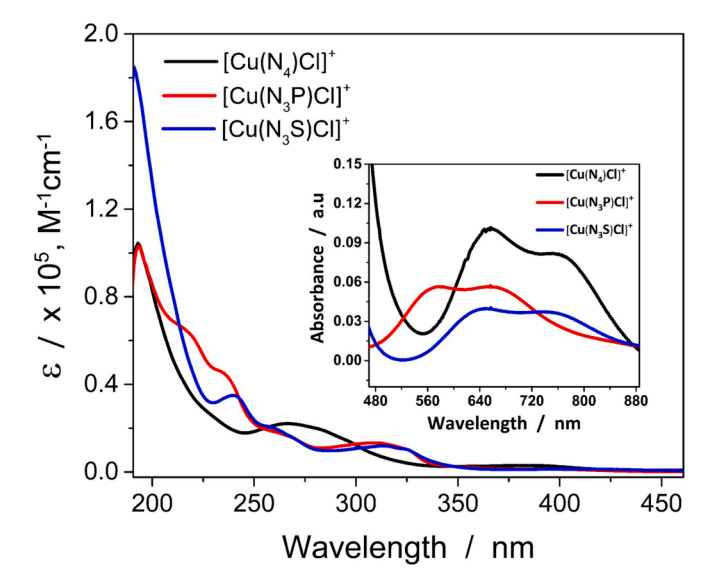


Fig. 2. UV–Vis absorption spectra of $[Cu(N_4)CI]^+$ (black), $[Cu(N_3P)CI]^+$ (red), and $[Cu(N_3S)CI]^+$ (blue) in anhydrous acetonitrile. The d-d transitions are shown in the inset.

observed for each complex between 220 and 420 nm. These absorption bands are attributed to $\pi\text{-}\pi^*$ and $n\text{-}\pi^*$ transitions of the ligands which was confirmed by recording the UV–visible spectra of the free ligands in anhydrous acetonitrile (Fig. S19). Metal-to-ligand charge transfer (MLCT) bands are also observed between 390 and 420 nm [27]. [Cu(N₄) Cl] $^+$ and [Cu(N₃P)Cl] $^+$ have MLCT bands appearing at higher energy (393 nm, $\epsilon=2400~\text{M}^{-1}\text{cm}^{-1}$ and 394 nm, $\epsilon=1400~\text{M}^{-1}\text{cm}^{-1}$, respectively) while [Cu(N₃S)Cl] $^+$ has an LMCT band at lower energy (413 nm, $\epsilon=1100~\text{M}^{-1}\text{cm}^{-1}$) [18,48–50]. We note that no emission was observed in the luminescence spectra of the complexes, which were recorded at 0.5 mM concentrations in N₂-saturated anhydrous CH₃CN solutions.

2.4. Electrochemistry

The redox properties of each complex were investigated by cyclic voltammetry in acetonitrile (CH $_3$ CN) solutions containing 0.1 M Bu $_4$ NPF $_6$ as the supporting electrolyte to assess the electronic effects associated with the equatorial amine, phosphine, and thioether substitutions. Cyclic voltammograms (CVs) were also collected in dichloromethane (DCM) / 0.1 M Bu $_4$ NPF $_6$ solutions to investigate the redox behavior in a non-coordinating solvent. CVs of the Cu^{II/I} process of each compound are shown in Fig. 3 and summarized in Table 2.

The scan rate dependence of the redox process was investigated, and plots of the anodic and cathodic peak currents versus the square root of the scan rate show a linear relationship consistent with diffusion-controlled, homogeneous redox behavior (Figs. S20-23) [51]. Consecutive cycles were recorded for each complex, which show CVs that are essentially unchanged during redox cycling, suggesting that irreversible ligand loss does not occur under these conditions on this timescale.

Large peak-to-peak separations (ΔE) for the Cu^{II/I} couples are observed and the ratios of the anodic and cathodic peak currents ($i_{p,a}/i_p$, $_c$) are far from unity for the [Cu(N₃L)Cl]⁺ series. The ΔE values range from 550 to 1000 mV. We note that the expected peak splitting value for a reversible one-electron redox process under standard conditions is \sim 59 mV [51]. These results indicate sluggish electron transfer kinetics at the electrode surface that presumably arise from large inner-sphere reorganization energies associated with the change in oxidation state.

[Cu(N₃P)Cl] ⁺ has the most positive Cu^I-to-Cu^{II} oxidation (0.58 V in CH₃CN and 0.28 V in DCM) within the series, which reflects the higher thermodynamic stability of this Cu^I species relative to the N₄ and N₃S copper complexes. Indeed, metal–ligand backbonding between the Cu ion and the equatorial phosphine donor is expected to result in a more electrophilic metal center. In CH₃CN, its oxidation potential is 420 and 390 mV more positive than the amine- and thioether-substituted compounds, respectively. In addition to this oxidation, a single prominent reduction is observed. In DCM, the oxidation potential, $E_{\rm pl,a}$, for [Cu (N₃P)Cl] ⁺ is 300 mV less positive than in CH₃CN and the peak splitting between its most prominent oxidation and reduction waves (ΔE) is lower at 730 mV compared to 1000 mV in CH₃CN. The more positive oxidation potential and larger peak splitting value observed in CH₃CN may be the result of reversible binding of solvent during the Cu^{II/I} redox process.

Smaller peak splitting values (ΔE) are observed for [Cu(N₄)Cl] ⁺ and [Cu(N₃S)Cl] ⁺, which are similar to one another and do not vary significantly between solvents. These values indicate greater reversibility of their Cu^{II/I} redox couples relative to that of the N₃P Cu complex. The oxidation potential ($E_{p1,a}$) of [Cu(N₃S)Cl] ⁺ is more positive than that of [Cu(N₄)Cl] ⁺ by 30 mV in CH₃CN and by 90 mV in DCM solution, which is consistent with the redox behavior reported by Lee *et al.* where copper complexes supported by tripodal tetradentate N₃S ligands exhibited more positive redox potentials relative to their N₄ counterparts [26]. Although the redox potentials of these complexes do not vary significantly in going from CH₃CN to DCM solutions, the CVs are more complex than the N₃P analogue.

Each of the complexes has a prominent reduction at approximately

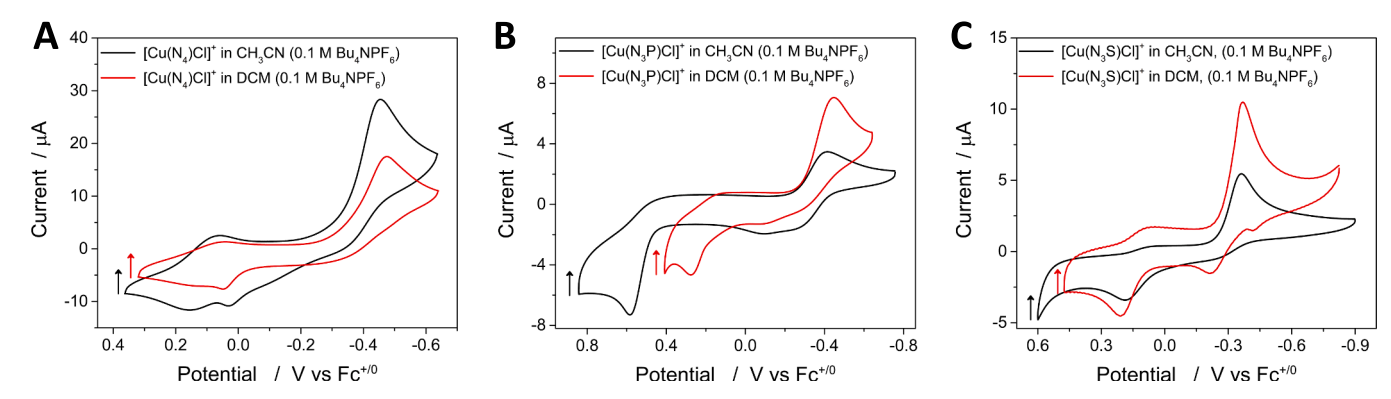


Fig. 3. Cyclic voltammograms of $[Cu(N_4)Cl]^+$ (A), $[Cu(N_3P)Cl]^+$ (B), and $[Cu(N_3S)Cl]^+$ (C) at 0.5 mM concentrations obtained under N_2 atmosphere in acetonitrile (CH₃CN) or dichloromethane (DCM) solutions containing 0.1 M Bu₄NPF₆ as specified in the legends. Glassy carbon working electrode, scan rate (v) = v00 mV/s

Table 2 Redox properties of the $[Cu(N_3L)Cl]^+$ complexes. [a]

Solvent / supporting electrolyte	Complexes	Redox potentials			
		$E_{p1,a}$	$E_{p1,c}$	$E_{p2,c}$	ΔE ^[b]
CH ₃ CN / 0.1 M Bu ₄ NPF ₆	[Cu(N ₄)Cl] +	0.16	0.06	-0.45	0.61
	[Cu(N ₃ P)Cl] +	0.58	-	-0.42	1.00
	[Cu(N ₃ S)Cl] +	0.19	0.07	-0.36	0.55
DCM / 0.1 M Bu ₄ NPF ₆	[Cu(N ₄)Cl] +	0.12	0.04	-0.47	0.59
	[Cu(N ₃ P)Cl] +	0.28	_	-0.45	0.73
	[Cu(N ₃ S)Cl] +	0.21	0.05	-0.41	0.62

[a] From CVs obtained with glassy carbon disk working electrode at $\upsilon=100$ mV/s. Potentials are in V versus $Fc^{+/0}$ and rounded to the nearest 0.01 V. [b] ΔE corresponds to peak splitting value between largest oxidation wave and largest reduction wave.

-0.4 V $(E_{p2,c})$. However, a smaller and more positive reduction event $(E_{p1,c})$ is also observed with the N₄ and N₃S complexes. This reduction wave $(E_{p1,c})$ of $[\mathbf{Cu(N_3S)Cl}]^+$ is not as conspicuous as it is for $[\mathbf{Cu(N_4)Cl}]^+$, but it becomes more prominent at faster scan rates (Fig. S20). Interestingly, apart from the prominent oxidation $(E_{p1,a})$, the other redox events have similar potentials, suggesting that electronically similar intermediates are generated upon reduction (*vide infra*).

2.5. UV-Visible spectroelectrochemistry

UV–Vis spectroelectrochemistry (SEC) was performed to gain insight into the structural/spectroscopic changes associated with the $\mathrm{Cu^{II/I}}$ redox process. The experiments were performed in DCM containing 0.1 M $\mathrm{Bu_4NPF_6}$; spectral changes are shown in Fig. 4. Notably, the UV–Vis spectral features, including the d-d transitions, of the complexes in DCM

are very similar to the spectral features observed in CH_3CN (Fig. 2), confirming that the solution structures of the complexes are not solvent dependent as seen in Fig. S18.

At resting potential in DCM, $[Cu(N_4)CI]^+$ shows two strong absorption bands at 223 and 265 nm, a moderate intensity band at 367 nm and lower intensity bands due to d-d transitions at 647 and 770 nm. With an applied potential corresponding to the peak current of the $Cu^{II/I}$ reduction, the d-d absorption bands decay, consistent with a metal-based reduction involving Cu^{II} (d⁹) to Cu^{I} (d¹⁰), and a new absorption band appears at 244 nm along with a weak band at 326 nm. Upon oxidation back to Cu^{II} , the original spectrum was recovered to \sim 50% of its initial absorbance (Fig. 4A, see inset).

Similar behavior was observed with $[Cu(N_3P)Cl]^+$ and $[Cu(N_3S)]$ Cl] +. In the case of [Cu(N₃P)Cl] +, disappearance of the d-d transition bands ($\lambda_{max} = 574$ and 658 nm), along with the charge transfer band at 400 nm, was observed when reducing potential was applied. The Cu¹ species with an absorption band at 265 nm, a moderate intensity band at 290 nm, and a shoulder at 320 nm was observed. Oxidation, in this case, fully restored the spectrum of the pristine Cu^{II} complex (Fig. 4B). [Cu (N₃S)Cl] + showed analogous spectral changes, where d-d transitions $(\lambda_{max}=657 \text{ and } 743 \text{ nm})$ and the charge transfer band at 423 nm disappeared under reducing conditions, giving rise to a new band at 260 nm. Again, oxidation back to Cu^{II} reinstated the original spectrum (Fig. 4C). The (quasi)reversible reduction-oxidation of the Cu complexes in the UV-Vis SEC studies indicate that these complexes are stable with respect to disproportionation. We note that loss of the d-d transitions upon reduction to the d¹⁰ Cu^I species limits the structural information that can be gained from the absorbance spectrum and thus SEC experiments in CH₃CN were not conducted.

In Cu compounds with multidentate ligands, the geometric constraint imposed by the ligand may favor the preferred geometry of

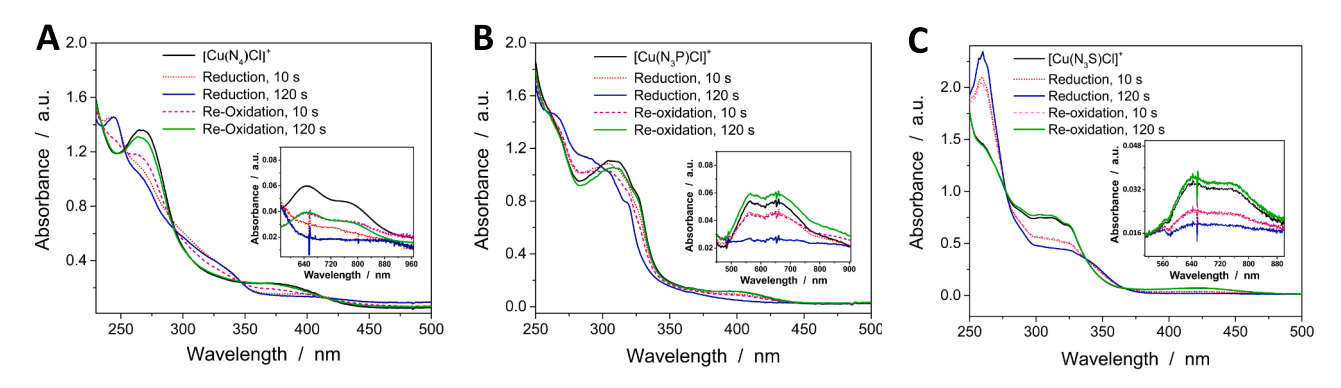


Fig. 4. UV–Vis SEC spectra of $[Cu(N_4)Cl]^+$ (A), $[Cu(N_3P)Cl]^+$ (B), and $[Cu(N_3S)Cl]^+$ (C). The d-d transitions are shown in the insets.

one oxidation state over the other. In such cases, changes in the metal oxidation state may be accompanied by large configurational changes as the ligand is poorly equipped to accommodate the preferred geometry of the new oxidation state. Indeed, the UV-Vis SEC experiments of each complex reveal significant differences in the chemical reversibility associated with redox changes at the metal center. [Cu(N₃S)Cl] + and [Cu(N₃P)Cl] + have intermediate geometries between the ideal square pyramidal and trigonal bipyramidal geometries with τ values of 0.54 and 0.56, respectively. The complete recovery of their spectral features following reduction to Cu^I and oxidation back to Cu^{II} indicate that these ligands can effectively support both oxidation states; the complexes do not undergo irreversible chemical reactions during the redox process. In contrast, as the τ value increases to 0.67 for $[Cu(N_4)Cl]^+$, the chemical reversibility is relatively low and $\sim 50\%$ of the initial spectrum is recovered. These results suggest that the more distorted or intermediate the imposed geometry is between square pyramidal and trigonal bipyramidal, the more chemically reversible the Cu^{II/I} redox process is within this series. We note that an alternative explanation is also plausible. From the ligand series, N₄ contains a hydrogen-bond donor while the N₃P and N₃S ligands do not. It has been shown that hydrogen bonding interactions in other first-row transition metal complexes can induce halide loss from the metal center [52]. In this case, the amine donor is expected to engage in intermolecular hydrogen bonding with the chloride of another N₄ Cu complex, which may cause irreversible dissociation of the halide.

2.6. Electronic structure calculations

Next, the inner-sphere reorganization energy (λ) for the Cu^{II/I} redox process has been investigated computationally using density functional theory (DFT) with the PBE1PBE (PBE0) functional, the 6-31G(d) basis set for all atoms save for def2TZVP for Cu, and an implicit solvation model. Here, λ denotes the difference in the energy between the optimized Cu^{II} oxidation state geometry and that of the Cu^{II} oxidation state computed at the Cu^I optimized geometry [53]. Another set of computations has also been performed utilizing a single molecule of acetonitrile (CH₃CN) added to a given Cu complex in order to probe explicit solvation within the implicit solvation model (see experimental section for more details).

Within the purely, fully implicit solvation computations, the [Cu $(N_3S)CI]^{+/0}$ structures in both Cu oxidation states have 5-coordinate geometries that resemble its crystal structure in Fig. 1. This produces a λ value of 0.34 eV, which is the lowest within the series as shown in Table 3. On the contrary, the apical quinoline donor de-coordinates from [Cu(N₃P)Cl] + upon reduction to give a four-coordinate geometry. Thus, $[Cu(N_3P)Cl]^+$ has a higher λ value due to the reorganization energy associated with decoordination. Similarly, the [Cu(N₄)Cl] + structure is also 5-coordinate, but upon reduction to the neutral Cu^I species, dissociation of the apical quinoline nitrogen donor is observed along with loss of the secondary amine donor from the equatorial position to give a 3-coordinate species. The large reorganization associated with this $Cu^{II/I}$ redox process produces a much larger λ value of 0.89 eV. The loss of an apical donor has been pointed out previously by Liu et al. during reduction of 5-coordinate Cu^{II} complexes to Cu^I compounds [54]. Donor dissociation in Cu(N₄)Cl may be due to the strain that is present in the angle formed between the secondary amine donor, the copper center, and the apical quinoline donor (L_{eq} -Cu- $N_q = 82.15^{\circ}$), which deviates significantly from the ideal TBP value of 90°. The computed λ

Table 3 Reorganization energies (λ in eV) using two different solvation models.

Compounds	Fully Implicit	Implicit with One Explicit CH ₃ CN
[Cu(N ₄)Cl] ⁺	0.89	1.20
[Cu(N ₃ P)Cl] ⁺	0.51	0.56
[Cu(N ₃ S)Cl] ⁺	0.34	1.05

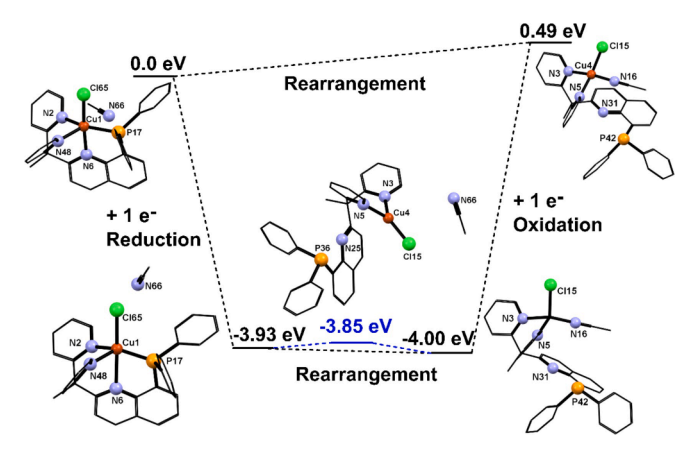
values have a direct correlation to the experimentally-derived τ values where the reorganization energy is less for the most distorted <code>[Cu(N_3S)CI]^+</code> complex having a τ value of 0.54 followed by <code>[Cu(N_3P)CI]^+</code> ($\tau=0.56)$ and then <code>[Cu(N_4)CI]^+</code> ($\tau=0.67)$. With a lower reorganization energy for <code>[Cu(N_3S)CI]^+</code>, the N₃S ligand is evidently able to better stabilize both oxidation states of the Cu center in comparison to its counterparts.

Inclusion of a single CH₃CN solvent molecule (while still maintaining the implicit solvation) in these computations involves considerable geometric changes and thus larger λ values with the exception of [Cu (N₃P)Cl] + which remains very similar. Indeed, [Cu(N₃P)Cl] + retains a 5-coordinate geometry resembling its solid-state structure while the added CH₃CN remains non-coordinated at a distance of 4.187 Å from the Cu center. In contrast, 5-coordinate structures are calculated for the [Cu $(N_4)Cl$] + and $[Cu(N_3S)Cl]$ + cations except that the equatorial L_{eq} donor is replaced with the explicit CH₃CN to produce a distorted SP geometry around the metal center. In the case of [Cu(N₄)Cl]⁺, the amine donor remains non-coordinated at a distance of 2.544 Å from the Cu center, Similarly in [Cu(N₃S)Cl]⁺, the thioether donor remains noncoordinated at a distance of 2.827 Å from the Cu center. Computations involving the Cu^I states of Cu(N₄)Cl and Cu(N₃S)Cl produce lower coordinate geometries with inclusion of an explicit CH₃CN molecule. This can be seen in the much larger λ values of 1.20 and 1.05 eV, respectively (Table 3). Both complexes undergo dissociation of the bidentate quinoline-Leg fragment, but Cu(N4)Cl produces a 3-coordinate Cu compound, and Cu(N₃S)Cl results in a 4-coordinate Cu species where the fourth ligand is CH₃CN.

The possibility of chloride (Cl⁻) loss from the Cu¹ center was also considered computationally. The computational results suggest that chloride dissociation from the Cu¹ state is an uphill process for all three complexes and, thus, thermodynamically unfavorable. In these calculations, chloride was removed from the one-electron reduced species in the presence of an explicit CH₃CN and the difference in energy was determined while taking into account the energy of the chloride ion itself. The energies associated with removal of the chloride ligand from the neutral Cu(N₄)Cl, Cu(N₃P)Cl, and Cu(N₃S)Cl species are 1.45, 0.20, and 0.52 eV higher than the chlorido-bound species, respectively.

The full energy profiles of all three complexes in the presence of a single, explicit CH_3CN have been computed. $[Cu(N_3P)Cl]^+$ in the presence of a single, explicit acetonitrile is multifaceted in that it exhibits a 4-coordinate, lowest energy compound that adopts a tetrahedral geometry, along with two other intermediates. One of these is a 3-coordinate Cu compound in a trigonal planar geometry with a non-covalent CH₃CN on the exterior of the molecule. The other species has a 5-coordinate structure similar to that of the initial Cu^{II} complex. The 3-coordinate and 5-coordinate Cu^I compounds lie 0.15 and 0.07 eV higher in energy than the 4-coordinate species. Hence, these are all very close in energy to one another. Even so, the steric bulk of the additional phenyl group in [Cu(N₃P)Cl] + likely hinders the coordination of CH₃CN to the Cu atom. Also, since the 5-coordinate neutral compound is found to be a minimum, unlike with the N₄ and N₃S Cu complexes, this species will be present in solution simultaneously with the intermediates containing a partially dissociated N₃P ligand.

Based on these computations, proposed changes in the inner-coordination sphere of the complexes associated with the $\text{Cu}^{II/I}$ redox processes are illustrated in Scheme 2 for $[\text{Cu}(\text{N}_3\text{P})\text{Cl}]^+$ and Schemes S1-S2 for the N₄ and N₃S derivatives. Similar schemes have been proposed for $\text{Cu}^{II/I}$ systems in the literature [55–57]. The relative energies in Scheme 2 are with respect to $[\text{Cu}(\text{N}_3\text{P})\text{Cl}]^+$. The $[\text{Cu}(\text{N}_3\text{P})\text{Cl}]^+$ complex upon 1e^- reduction forms a 5-coordinate neutral compound which has an energy of -3.93 eV relative to the initial Cu^{II} species. The 5-coordinate Cu^{I} species is a 20-electron coordination complex. This 5-coordinate species, thus, rearranges to either a 3-coordinate compound (16-electron complex) at -3.85 eV or a 4-coordinate compound (18-electron complex), which is the minimum at -4.00 eV. We propose that the 4-coordinate species undergoes 1e^- oxidation to a 4-coordinate



Scheme 2. Computed structures and their relative energies associated with the $Cu^{II/I}$ oxidation states of $[Cu(N_3P)Cl]^+$ with an explicit CH_3CN .

 ${\rm Cu^{II}}$ complex, which has a relative energy of 0.49 eV. The 4-coordinate ${\rm Cu^{II}}$ complex can then convert back to the initial ${\rm [Cu(N_3P)Cl]}^+$ species upon dissociation of ${\rm CH_3CN}$, similar to the dynamic coordination-decoordination behavior observed by Leandri *et al.* during redox cycling of a homoleptic ${\rm Cu(II)}$ dimine complex [58]. The presence of multiple structures at similar energies during the redox process may explain the sluggish electron transfer kinetics observed by cyclic voltammetry for ${\rm [Cu(N_3P)Cl]}^+$ in ${\rm CH_3CN}$.

As stated earlier, the [Cu(N₄)Cl] + and [Cu(N₃S)Cl] + complexes do not show multiple species in solution upon 1e reduction, but they undergo partial ligand dissociation to give a neutral 3-coordinate Cu(N4)Cl species (16-electron complex) and a neutral 4-coordinate Cu(N3S)Cl species (18-electron complex). The neutral Cu(N₄)Cl compound adopts a trigonal planar geometry with two pyridyl donors (N_{pv}) and a chlorido donor and has an energy of -4.33 eV relative to the Cu^{II} species. We propose that the 3-coordinate Cu^I species undergoes 1e⁻ oxidation to a 4coordinate CH₃CN-bound Cu^{II} complex that adopts a square planar geometry, which has a relative energy of 0.01 eV. The energy difference between the initial 5-coordinate Cu^{II} species and this 4-coordinate Cu^{II} complex suggests dynamic coordination-decoordination behavior is likely in solution at room temperature. On the contrary, neutral compound Cu(N₃S)Cl has an energy of -4.38 eV relative the initial Cu^{II} species and adopts a tetrahedral geometry with two pyridyl donors (N_{pv}), a chlorido donor, and an explicitly added CH₃CN solvent molecule. We propose that the 4-coordinate neutral species undergoes 1eoxidation to a 4-coordinate Cu^{II} cation which is at an energy of -0.12 eV relative to the 5-coordinate Cu^{II} cation. The 4-coordinate Cu^{II} cation adopts a square planar geometry. The large λ values obtained for [Cu (N₄)Cl] + and [Cu(N₃S)Cl] + are, thus, due to significant geometric changes. The geometric changes observed among all three complexes are consistent with the usual geometries adopted by Cu^{II} and Cu^I compounds as discussed in the introduction.

The computational results using an explicit CH_3CN within the implicit solvation model provide key insights into the experimental results of the complexes obtained in solution. First, the UV–visible spectra of $[Cu(N_4)Cl]^+$ and $[Cu(N_3S)Cl]^+$ in acetonitrile appear to favor distorted square pyramidal geometries in solution, which is supported by the computed 5-coordinate Cu^{II} ions obtained by DFT calculations where the equatorial N- or S-donor (L_{eq}) , respectively, is replaced by CH_3CN . The UV–visible spectrum of $[Cu(N_3P)Cl]^+$ denotes an intermediate geometry as expected from its solid-state structure where the phosphine donor remains bound as determined computationally. Next, the calculations indicate that the difference in energy between the 5-coordinate Cu^{II} cation and the 4-coordinate Cu^{II} cation following the redox process for each system is small for $[Cu(N_4)Cl]^+$ (0.01 eV) and $[Cu(N_3S)Cl]^+$ (0.12 eV), and relatively large for $[Cu(N_3P)Cl]^+$ (0.49 eV). These results suggest that thermally accessible equilibria are likely at room

temperature, particularly for the N₄ and N₃S copper complexes, to give multiple species in solution. The observation of additional reduction and oxidation waves in CVs of [Cu(N₄)Cl] + and [Cu(N₃S)Cl] + is rationalized by the presence of energetically similar 4-coordinate and 5-coordinate Cu^{II} species with thermally accessible isomerization energies in contrast to the greater energy difference and less complex cyclic voltammetry of [Cu(N₃P)Cl] +. Finally, the similarity in redox potentials for all but the most positive oxidation wave (Table 2) points to electronically similar intermediates following 1e- reduction of the complexes. Indeed, the computations predict dissociation of the equatorial donor Leg, along with the quinoline donor, for all three complexes, to ultimately generate a 4-coordinate intermediate with two pyridines, a chloride, and an acetonitrile coordinated to the metal. The disparate L_{eq} donors that differentiate the complexes from one another are not coordinated in several of the computationally-predicted intermediates across the series and, thus, will have a small influence on the associated Cu^{II/I} redox potentials.

3. Conclusion

Three new rigid tetradentate ligands of N_4 , N_3P , and N_3S coordination pockets and their corresponding Cu^{II} complexes have been synthesized and characterized. Solid-state structures and electrochemical analysis demonstrate that the change in the equatorial donor alters the geometry and redox properties of the complexes. Distorted geometries are observed across the series that favor, even if slightly, trigonal bipyramidal geometries as the geometric index τ is greater than 0.5 for each complex.

UV–visible measurements in acetonitrile indicate that the N_3P complex prefers an intermediate geometry consistent with its crystal structure and DFT optimized geometry, while the N_4 and N_3S complexes favour, albeit slightly for the N_3S complex, distorted square pyramidal geometries in solution. Given the rigidity of the tetradentate framework, this may entail partial ligand dissociation and acetonitrile binding as found computationally. In cyclic voltammograms, large peak-to-peak separations (ΔE) are observed that suggest large inner-sphere reorganization energies are associated with the $Cu^{II/I}$ redox couple. The peak splitting values decrease in cyclic voltammograms collected in noncoordinating dichloromethane solutions, lending support to the hypothesis that coordinating solvents such as CH_3CN bind to the metal center during the redox process. Dynamic coordination-decoordination behavior is proposed and supported by the results of the density functional theory calculations.

Spectroelectrochemical experiments reveal that the chemical reversibility of each system is closely tied to the nature of each ligand. It is not clear if the observed reversibility in SEC experiments is associated with the ability of the ligand to accommodate both the Cu^I and Cu^{II} oxidation states of the metal, or the presence/absence of a hydrogenbond donor in the ligand scaffold. In this context, the N_3S and N_3P complexes exhibit good stability upon redox cycling, as measured by UV–visible spectral changes, which have more intermediate geometries and no hydrogen bond donor functionality. The geometry of the N_4 complex, on the other hand, favors the ideal TBP geometry more and has the potential for H-bonding interactions via the N—H moiety of the L_{eq} amine donor.

Given the observations reported herein, this series of ligands offers preorganized metal binding pockets to explore bioinspired Cu coordination chemistry. These complexes are relevant to the active sites of Class III T1Cu enzymes such as azurin that have distorted trigonal bipyramidal geometries. However, without the constraint imposed by the protein scaffold, significant structural rearrangement and large reorganization energies are observed with these molecular systems.

4. Experimental section

4.1. Materials and methods

All reported synthetic manipulations were carried out using standard Schlenk techniques or in an MBraun glovebox under nitrogen atmosphere. Acetonitrile (CH₃CN) and 1,4-dioxane were freshly distilled beforehand for synthesis and electrochemistry. Tetrahydrofuran (THF), dichloromethane (DCM), toluene, and diethyl ether were dried with a Pure Process Technology solvent purification system. 1,1'-bis(diisopropylphosphino)ferrocene (DiPPF), diphenylphosphine, and anhydrous copper(II) chloride were purchased from Strem Chemicals, Inc. All other chemicals were reagent or ACS grade, purchased from commercial vendors, and used without further purification. ¹H, ³¹P, and ¹³C NMR spectra were obtained using Bruker spectrometers operating at 400 MHz or 300 MHz (¹H), 133 MHz or 100 MHz (³¹P), and 100 MHz or 75 MHz (13C) as specified. Spectra were calibrated versus residual protiated solvent peaks. Chemical shifts are reported in parts per million (ppm). High-resolution electrospray ionization mass spectra (HR-ESI-MS) were obtained with a Waters SYNAPT HDMS Q-TOF mass spectrometer and elemental analyses of carbon, hydrogen, and nitrogen were conducted by Atlantic Microlab, Inc., Norcross, Georgia. UV-Vis spectra were recorded on an Agilent Technologies Cary 8454 UV-Visible Spectrophotometer equipped with a diode-array detector.

4.2. Electrochemical measurements

Cyclic voltammetry experiments were performed with a typical three-electrode set-up using a CH Instruments 600E Series potentiostat. The electrochemical cell was equipped with a glassy carbon disk working electrode (CH Instruments, 3 mm diameter), a platinum wire counter electrode, and a silver wire quasi-reference electrode. CH $_3$ CN or DCM solutions containing 0.1 M Bu $_4$ NPF $_6$ as the supporting electrolyte were used in electrochemical studies. Ferrocene was used as an internal standard to reference the potential and added at the end of each experiment. Freshly-made solutions were thoroughly degassed with nitrogen for 10 min prior to each experiment.

4.3. Quantum chemical computations

Quantum chemical computations utilizing density functional theory (DFT) with the PBE1PBE (PBE0) functional [59,60] are employed along with a mixed 6-31G(d) and Def2TZVP basis set [61–63]. The latter is for Cu and the former for all other atoms in a manner similar to that for other, related Cu complexes [53]. The Gaussian16 program [64] is employed for all quantum chemical computations. A polarized continuum model simulates the solvation environment for acetonitrile. The reorganization energy (λ) is computed here and defined as the difference in the energy between the +2 oxidation state of the Cu atom computed at the +1 optimized geometry and the total electronic energy at the optimized +2 oxidation state geometry [65]. In addition, another set of computations utilizes a single molecule of acetonitrile (CH₃CN) added to a given Cu complex in order to probe explicit solvation within the implicit solvation model.

4.4. UV-Vis spectroelectrochemical (UV-Vis SEC) measurements

UV-Vis SEC measurements were performed in a Honeycomb thinlayer spectroelectrochemical cell purchased from Pine Research Instrumentation. The cell comprises a thin-layer quartz cuvette and a honeycomb electrode card, and a Ag wire quasi-reference electrode. The electrode card is composed of an onboard Au working and a Pt counter electrode. Prior to each measurement, the cell was filled with freshly made catalyst solution (0.5 mM catalyst in DCM / 0.1 M $\rm Bu_4NPF_6$), thoroughly degassed with nitrogen and sealed from atmosphere. A potentiostat was connected to the cell to perform cyclic voltammetry and bulk electrolysis while the spectral changes were monitored by the UV–Vis Spectrophotometer. The reported spectra were obtained by performing short-term bulk electrolyses (greater than 120 $\it sec$) at different potential regions of the CVs.

4.5. Ligand synthesis

1,1-bis(2-pyridyl)ethane (1) [28] and 2,8-dibromoquinoline (2) [29,66] were synthesized as previously reported. Ligand precursor 8-bromo-2-(1,1-di(pyridin-2-yl)ethyl)quinoline (3) was prepared by reacting 1 with *n*-butyllithium prior to reacting the lithiated intermediate with 2. Final ligands were obtained by palladium-catalyzed coupling reactions following modified procedures [60,61].

8-bromo-2-(1,1-di(pyridin-2-yl)ethyl)quinoline, 3. Under N2 atmosphere, a solution of 1 (1.284 g, 7.000 mmol) in 30 mL of THF was cooled to -78 °C, followed by slow addition of 1.6 M n-butyllithium in hexanes (5.25 mL, 8.400 mmol). The resultant mixture was stirred for 45 min. The electrophile 2 (2.000 g, 7.000 mmol) in 10 mL THF was added dropwise to the lithiated solution using a syringe. The cooling bath was removed and the reaction mixture was allowed to reach room temperature and then was refluxed for 72 h. The mixture was cooled to room temperature followed by addition of cold water. The organic layer was separated and the aqueous layer was extracted three times with diethyl ether. All the organic phases were combined and the volume was reduced in vacuo to obtain an oily residue. Hexane (20 mL) was added to this oily residue and the mixture was stirred overnight. The solid compound formed was filtered and dried in vacuo to get compound 3 in 79% yield (2.144 g). ¹H NMR (acetone- d_6 , 400 MHz): δ 8.48 (m, J = 1.64 Hz, J = 1.9 Hz, 2H, 8.17 (d, J = 8.6 Hz, 1H), 7.92 (d, J = 8.12 Hz, 1H), 7.71(m, 2H), 7.47 (m, 2H), 7.26 (d, J = 7.96 Hz, 2H), 7.21 (t, J = 5.6 Hz, 6.1)Hz, 2H), 2.44 (s, 3H). 13 C NMR (acetone- d_6 , 100 MHz): δ 167.83, 166.92, 149.48, 136.97, 136.13, 133.59, 129.17, 128.52, 127.79, 125.87, 125.39, 124.39, 122.35, 62.12, 27.65. HR-ESI-MS (M⁺) m/z calc. for $[3 + H^+]$, 390.0606, Found, 390.0559.

2-(1,1-bis(2-pyridyl)ethyl)-N-phenylquinolin-8-amine, N₄. In a glovebox, an oven-dried pressure flask was charged with 2 (0.350 g, 0.897 mmol), Pd₂(dba)₃ (0.029 g, 0.031 mmol), rac-BINAP (0.045 g, 0.073 mmol), NaO^tBu (0.180 g, 1.872 mmol), and anhydrous toluene (20 mL). The mixture was stirred for 30 min followed by addition of aniline (0.125 g, 1.345 mmol) and the flask was sealed with a Teflon cap. The flask was brought out of the glovebox and heated at 120 $^{\circ}$ C for 48 h. The reaction mixture was cooled to room temperature and diluted with dichloromethane (20 mL). The contents were filtered through a pad of silica and the organic volatiles were removed in vacuo. The title compound was purified as a light-yellow solid by silica gel column chromatography eluting with 1:1 hexane: ethyl acetate (0.350 g, 87%). ¹H NMR (CD₃CN, 400 MHz): δ 8.51 (dq, J=1 Hz, J=4.72 Hz, 2H), 8.11 (d, J = 8.68 Hz, 1H, 7.92 (s, 1H), 7.69 (td, J = 7.78, 1.89 Hz, 2H), 7.46, (m, 1.89 Hz)1H), 7.44, (m, 1H), 7.40 (t, J = 7.86 Hz, 1H), 7.34 (t, J = 7.94 Hz, 2H), 7.26 (m, 2H), 7.23 (m, 3H), 7.21 (m, 2H), 6.99 (t, J = 7.32, 1H), 2.39 (s, 3H). ¹³C NMR (CD₃CN, 101 MHz): δ 166.74, 164.48, 149.34, 142.87, 140.41, 137.24, 136.93, 136.70, 130.33, 128.06, 127.96, 124.64, 123.95, 122.59, 122.55, 122.47, 119.84, 119.72, 117.37, 108.91, 61.58, 27.34. HR-ESI-MS (M⁺) m/z calc. for [N₄ + H⁺], 403.1923, Found

2-(1,1-bis(2-pyridyl)ethyl)-8-(diphenylphosphaneyl)quinoline, N_3P . In a glovebox, an oven-dried pressure flask was charged with 2 (0.400 g, 1.025 mmol), $Pd(OAc)_2$ (0.012 g, 0.051 mmol), and 1,1'-bis

(diisopropylphosphino)ferrocene (0.026 g, 0.062 mmol). Then, 8 mL anhydrous toluene was added to the flask and the mixture was stirred for one hour. Diphenylphosphine (0.178 mL, 1.025 mmol) and NaO^tBu (0.118 g, 1.230 mmol) were added to the orange suspension and the flask was sealed with a Teflon cap. The flask was brought out of the glovebox and heated at 120 $^{\circ}\text{C}$ for 48 h. The reaction mixture was then cooled down to room temperature and solvent was removed in vacuo. The title compound was purified as a light-yellow solid by a deactivated silica column eluting with 2:1 hexanes:ethyl acetate (0.340 g, 67%). The product is air and moisture stable in the solid state. ¹H NMR (Acetone- d_6 , 300 MHz): δ 8.42–8.40 (m, 2H), 8.14 (d, J = 8.67 Hz, 1H), 7.88 (d, J = 8.1 Hz, 1H), 7.54 (td, J = 1.89 Hz, J = 7.86 Hz, 2H), 7.47–7.40 (m, 2H), 7.35-7.28 (m, 6H), 7.26-7.20 (m, 4H), 7.15-7.11 (m, 2H), 7.01–6.97 (m, 1H), 6.88 (br d, J = 8.04 Hz, 2H), 2.04 (s, 3H). ¹³C NMR (acetone- d_6 , 100 MHz): δ 166.82 (s), 165.45 (s), 149.09 (s), 148.48 (d), 140.04 (d), 139.15 (d), 136.60 (s), 135.90 (s), 135.10 (s), 134.89 (s), 133.82 (s), 132.54 (d), 129.20 (t), 128.99 (s), 127.16-127.09 (m), 124.26–124.17 (m), 121.88 (s), 61.82 (s), 27.37 (s). ³¹P NMR (CDCl₃, 167 MHz) δ -12.35. HR-ESI-MS (M⁺) m/z calc. for [N₃P + H⁺], 496.1943, Found, 496.1937.

2-(1,1-bis(2-pyridyl)ethyl)-8-(phenylthio)quinoline, N₃S. In a glovebox, an oven-dried pressure flask was charged with 2 (0.350 g, 0.897 mmol), Pd(OAc)₂ (0.010 g, 0.045 mmol), and 1,1'-bis(diisopropylphosphino)ferrocene (0.023 g, 0.054 mmol). Then, 8 mL anhydrous 1,4-dioxane was added to the flask and the mixture was stirred for one hour. Thiophenol (0.092 mL, 0.897 mmol) and NaO^tBu (0.104 g, 1.076 mmol) were added to the orange suspension and the flask was sealed with a Teflon cap. The flask was brought out of the glovebox and heated at 115 °C for 48 h. The reaction mixture was then cooled to room temperature and solvent was removed in vacuo. The desired product was purified by a short silica plug and obtained as a light-yellow solid (0.342 g, 91%). The product is air and moisture stable in solid state. ¹H NMR (CD₃CN, 400 MHz): δ 8.49 – 8.46 (m, 2H), 8.10 (d, J = 8.72 Hz, 1H), 7.69–7.62 (m, 3H), 7.54–7.52 (m, 2H), 7.46–7.41 (m, 4H), 7.33 (t, J =7.92 Hz, 1H), 7.22 – 7.18 (m, 4H), 7.00 (dd, J = 1.17 Hz, J = 7.47 Hz, 1H), 2.33 (s, 3H). 13 C NMR (CD₃CN, 100 MHz): δ 166.79 (s), 165.81 (s), 149.35 (s), 143.97 (s), 140.39 (s), 137.08 (s), 136.28 (s), 135.73 (s), 133.55 (s), 130.69 (s), 129.65 (s), 127.55 (s), 127.44 (s), 126.59 (s), 125.44 (s), 124.68 (s), 124.45 (s), 122.44 (s), 61.86 (s), 27.56 (s). HR-ESI-MS (M⁺) m/z calc. for [N₃S + H⁺], 420.1534, Found: 420.1570.

4.6. Synthesis of the metal complexes

Common synthetic procedure. A methanolic (5 mL) solution of 0.050 g of the respective ligand was made in a 20 mL scintillation vial under N_2 atmosphere and 1 equivalent of anhydrous CuCl_2 was added. The mixture was stirred overnight at room temperature before the solvent was evaporated under reduced pressure. The resulting powder was washed with a small amount of diethyl ether and purified by crystallization.

 $\mbox{[Cu(N_4)Cl]}^+,\mbox{ [Cu(N_4)Cl](PF_6):}$ The complex was synthesized by reacting ligand N_4 (0.050 g, 0.101 mmol) and anhydrous \mbox{CuCl}_2 (0.014 g, 0.101 mmol) following the common procedure. After stirring overnight at room temperature, one equivalent of NaPF_6 was added to the reaction mixture, which was stirred for an additional 30 min. The solution was concentrated and the complex was purified on a Sephadex TM LH-20 column. Pure fractions collected from the column were combined and concentrated. The metal complex was precipitated by adding diethyl ether. The precipitate was collected on a glass frit and washed with diethyl ether and dried under vacuum. Yield = 0.060 g (75%). Elem. Anal. calc. for $\mbox{C}_{27}\mbox{H}_{22}\mbox{ClCuN}_4\mbox{PF}_6 \bullet (\mbox{CH}_3\mbox{CN}_0.5(\mbox{C}_4\mbox{H}_10\mbox{O}_{0.5}:\mbox{C}_5,\mbox{51.18};\mbox{ H},$

4.08, N, 8.95; Found: C, 51.40; H, 3.84; N, 8.96. HR-ESI-MS (M^+) m/z calc. for [Cu(N₄)Cl] $^+$, 500.0829. Found: 500.0824. Green, X-ray quality crystals of the chloride salt were grown from a concentrated solution of 3:1 acetonitrile:toluene by slow diffusion of diethyl ether at 8 °C.

[Cu(N₃P)Cl] $^+$, [Cu(N₃P)Cl](PF₆): The complex was prepared from ligand N₃P (0.050 g, 0.101 mmol) and anhydrous CuCl₂ (0.014 g, 0.101 mmol) following the common synthetic procedure. The blue powder of the chloride salt was re-dissolved in a minimum amount of water and excess aqueous NH₄PF₆ (5 eq.) was added dropwise to initiate metathesis. After stirring the suspension for 30 min, the precipitate was filtered, washed with a small amount of water and diethyl ether, and dried under vacuum. Dark blue crystals of the hexafluorophosphate (PF₆ $^-$) salt were grown from a concentrated solution of acetone by slow diffusion of diethyl ether at -20 °C. Yield = 0.067 g (90%). Elem. Anal. calc. for C₃₃H₂₆ClCuF₆N₃P₂•(CH₃)₂CO: C, 54.21; H, 4.04; N, 5.27. Found: C, 54.19; H, 4.07; N, 5.44. HR-ESI-MS (M⁺) m/z calc. for [Cu(N₃P)Cl]⁺, 593.0849. Found: 593.0855.

[Cu(N₃S)Cl] ⁺, [Cu(N₃S)Cl]Cl: The complex was synthesized by reacting ligand N₃S (0.050 g, 0.119 mmol) and anhydrous CuCl₂ (0.016 g, 0.119 mmol) following the common synthetic procedure. Yield = 0.068 g (86%). Elem. Anal. calc. for C₂₇H₂₁Cl₂CuN₃S•(H₂O)_{1.5}: C, 55.82; H, 4.16; N, 7.23. Found: C, 55.61; H, 4.10; N, 7.24. HR-ESI-MS (M⁺) m/z calc. for [Cu(N₃S)Cl]⁺, 517.0441. Found: 517.0417. Green, X-ray quality crystals of the PF₆[−] salt were grown from a concentrated solution of acetone by slow diffusion of diethyl ether at −20 °C.

CRediT authorship contribution statement

Anthony Devdass: Investigation, Formal analysis, Writing – original draft. Kallol Talukdar: Investigation, Formal analysis, Writing – original draft. Matthias Zeller: Investigation, Formal analysis. Ryan C. Fortenberry: Investigation, Formal analysis, Writing – review and editing. Jonah W. Jurss: Conceptualization, Formal analysis, Resources, Supervision, Project administration, Writing – review & editing.

Declaration of Competing Interest

The authors declare that they have no known competing financial interests or personal relationships that could have appeared to influence the work reported in this paper.

Acknowledgements

This material is based on work supported by the National Science Foundation under Grant No. 1757220. Acknowledgment is made to the donors of The American Chemical Society Petroleum Research Fund for partial support of this research (Grant No. 58707-DNI3). Funding for the single crystal X-ray diffractometer was made possible by the National Science Foundation through the Major Research Instrumentation Program under Grant No. 1625543.

Appendix A. Supplementary data

CCDC 2101121-2101123 contain the supplementary crystallographic data for the N_4 , N_3S , and N_3P copper(II) complexes, respectively. These data can be obtained free of charge via http://www.ccdc.cam.ac.uk/conts/retrieving.html, or from the Cambridge Crystallographic Data Centre, 12 Union Road, Cambridge CB2 1EZ, UK; fax: (+44) 1223–336-033; or e-mail: deposit@ccdc.cam.ac.uk. Supplementary data to this article can be found online at https://doi.org/10.1016/j.poly.2021.115558.

References

- [1] D.B. Rorabacher, Electron transfer by copper centers, Chem. Rev. 104 (2) (2004) 651–698, https://doi.org/10.1021/cr020630e.
- [2] P.J.M.W.L. Birker, J. Helder, G. Henkel, B. Krebs, J. Reedijk, Reedijk, Synthesis and spectroscopic characterization of copper(I) and copper(II) complexes with 1,6-bis (2-benzimidazolyl)-2,5-dithiahexane (BBDH). X-ray structure of trigonalbipyramidal coordinated [Cu(BBDH)CI]CI.2C2H5OH, Inorg. Chem. 21 (1) (1982) 357–363, https://doi.org/10.1021/ic00131a064.
- W. Kaim, J. Rall, Copper—a "Modern" Bioelement, Angewandte Chemie International Edition in English 35 (1) (1996) 43–60, https://doi.org/10.1002/ (ISSN)1521-377310.1002/anie.v35:110.1002/anie.199600431.
- [4] E.I. Solomon, U.M. Sundaram, T.E. Machonkin, Multicopper oxidases and oxygenases, Chem. Rev. 96 (7) (1996) 2563–2606, https://doi.org/10.1021/cr9500460
- [5] E.I. Solomon, M.J. Baldwin, M.D. Lowery, Electronic structures of active sites in copper proteins: contributions to reactivity, Chem. Rev. 92 (1992) 521–542, https://doi.org/10.1021/cr00012a003.
- [6] J.T. Rubino, K.J. Franz, Coordination chemistry of copper proteins: how nature handles a toxic cargo for essential function, Journal of Inorganic Biochemistry. 107 (2012) 129–143, https://doi.org/10.1016/j.jinorgbio.2011.11.024.
- [7] J.M. Moore, C.A. Lepre, G.P. Gippert, W.J. Chazin, D.A. Case, P.E. Wright, Highresolution solution structure of reduced French bean plastocyanin and comparison with the crystal structure of poplar plastocyanin, J. Mol. Biol. 221 (2) (1991) 533–555, https://doi.org/10.1016/0022-2836(91)80071-2.
- [8] G.V. Driessche, J.V. Beeumen, C. Dennison, A. Geoffrey Sykes, Heterogeneity of the covalent structure of the blue copper protein umecyanin from horseradish roots, Protein Sci. 4 (2) (1995) 209–227, https://doi.org/10.1002/pro.v4:210.1002/ pro 5550040208
- [9] C.W. Hoitink, G.W. Canters, The importance of Asn47 for structure and reactivity of azurin from Alcaligenes denitrificans as studied by site-directed mutagenesis and spectroscopy, J. Biol. Chem. 267 (20) (1992) 13836–13842, https://doi.org/ 10.1016/S0021-9258(19)49644-0
- [10] J. Richardson, K.A. Thomas, B.H. Rubin, D.C. Richardson, Crystal structure of bovine Cu, Zn superoxide dismutase at 3 A resolution: chain tracing and metal ligands, Proc. Natl. Acad. Sci. U. S. A. 72 (4) (1975) 1349–1353, https://doi.org/ 10.1073/pnas.72.4.1349.
- [11] H.D. Ellerton, N.F. Ellerton, H.A. Robinson, Hemocyanin—a current perspective, Prog. Biophys. Mol. Biol. 41 (1983) 143–247, https://doi.org/10.1016/0079-6107 (83)00028-7
- [12] J.M. Brown, L. Powers, B. Kincaid, J.A. Larrabee, T.G. Spiro, Structural studies of the hemocyanin active site. 1. Extended x-ray absorption fine structure (EXAFS) analysis, J. Am. Chem. Soc. 102 (12) (1980) 4210–4216, https://doi.org/10.1021/ ia00532a037
- [13] F. Fusetti, K.H. Schröter, R.A. Steiner, P.I. van Noort, T. Pijning, H.J. Rozeboom, K. H. Kalk, M.R. Egmond, B.W. Dijkstra, Crystal structure of the copper-containing quercetin 2,3-dioxygenase from Aspergillus japonicus, Structure. 10 (2) (2002) 259–268, https://doi.org/10.1016/S0969-2126(02)00704-9.
- [14] K.M. Lancaster, S.D. George, K. Yokoyama, J.H. Richards, H.B. Gray, Type-zero copper proteins, Nature Chem. 1 (9) (2009) 711–715, https://doi.org/10.1038/psperg. 412
- [15] K.M. Lancaster, M.-E. Zaballa, S. Sproules, M. Sundararajan, S. DeBeer, J. H. Richards, A.J. Vila, F. Neese, H.B. Gray, Outer-sphere contributions to the electronic structure of type zero copper proteins, J. Am. Chem. Soc. 134 (19) (2012) 8241–8253. https://doi.org/10.1021/j.30210108
- (2012) 8241–8253, https://doi.org/10.1021/ja302190r.
 [16] K.M. Lancaster, Copper Protein Variants: "Type Zero" Sites, in: Encyclopedia of Inorganic and Bioinorganic Chemistry, American Cancer Society, 2014: pp. 1–6. 10.1002/9781119951438.eibc2246.
- [17] K.D. Karlin, J.C. Hayes, Shi. Juen, J.P. Hutchinson, Jon. Zubieta, Tetragonal vs. trigonal coordination in copper(II) complexes with tripod ligands: structures and properties of [Cu(C21H24N4)Cl]PF6 and [Cu(C18H18N4)Cl]PF6, Inorg. Chem. 21 (1982) 4106–4108, https://doi.org/10.1021/ic00141a049.
- [18] A.W. Addison, P.J. Burke, K. Henrick, T.N. Rao, E. Sinn, Pentacoordinate copper complexes of nitrogen-sulfur donors: structural chemistry of two complexes of bis (2-(2-benzimidazoly))ethyl) sulfide with the sulfur alternatively in equatorial and axial coordination modes, Inorg. Chem. 22 (1983) 3645–3653, https://doi.org/ 10.1021/jc00166a030.
- [19] C. Place, J.-L. Zimmermann, E. Mulliez, G. Guillot, C. Bois, J.-C. Chottard, Crystallographic, electrochemical, and pulsed EPR study of copper(II) polyimidazole complexes relevant to the metal sites of copper proteins, Inorg. Chem. 37 (16) (1998) 4030–4039, https://doi.org/10.1021/ic9715660.
- [20] P.L. Holland, W.B. Tolman, A structural model of the type 1 copper protein active site: N2S(thiolate)S(thioether) ligation in a Cu(II) complex, J. Am. Chem. Soc. 122 (2000) 6331–6332, https://doi.org/10.1021/ja001328v.
- [21] M. Vaidyanathan, R. Balamurugan, U. Sivagnanam, M. Palaniandavar, Synthesis, structure, spectra and redox of Cu(II) complexes of chelating bis(benzimidazole)—thioether ligands as models for electron transfer blue copper proteins, J. Chem. Soc., Dalton Trans. (2001) 3498–3506, https://doi.org/10.1039/B103511H.
- [22] Z. Tyeklar, R.R. Jacobson, N. Wei, N.N. Murthy, J. Zubieta, K.D. Karlin, Reversible reaction of dioxygen (and carbon monoxide) with a copper(I) complex. X-ray structures of relevant mononuclear Cu(I) precursor adducts and the trans-(.mu.-1,2-peroxo)dicopper(II) product, J. Am. Chem. Soc. 115 (7) (1993) 2677–2689, https://doi.org/10.1021/ja00060a017.
- [23] S.Y. Shaban, F.W. Heinemann, R. van Eldik, A new trigonal-bipyramidal [CuII (pytBuN3)Cl2] complex: synthesis, structure and ligand substitution behaviour,

- Eur. J. Inorganic Chem. 2009 (2009) 3111–3118, https://doi.org/10.1002/eijc.200900302.
- [24] F. Champloy, N. Benali-Chérif, P. Bruno, I. Blain, M. Pierrot, M. Réglier, A. Michalowicz, Studies of copper complexes displaying N3S coordination as models for CuB center of dopamine β-hydroxylase and peptidylglycine α-hydroxylating monooxygenase, Inorg. Chem. 37 (16) (1998) 3910–3918, https://doi.org/10.1021/ic9709281.
- [25] L.Q. Hatcher, D.-H. Lee, M.A. Vance, A.E. Milligan, R. Sarangi, K.O. Hodgson, B. Hedman, E.I. Solomon, K.D. Karlin, Dioxygen reactivity of a copper(I) complex with a N3S thioether chelate; peroxo—dicopper(II) formation including sulfurligation, Inorg. Chem. 45 (25) (2006) 10055–10057, https://doi.org/10.1021/ic061813c
- [26] D.-H. Lee, L.Q. Hatcher, M.A. Vance, R. Sarangi, A.E. Milligan, A.A. Narducci Sarjeant, C.D. Incarvito, A.L. Rheingold, K.O. Hodgson, B. Hedman, E.I. Solomon, K.D. Karlin, Copper(I) complex O2-reactivity with a N3S thioether ligand: a copper—dioxygen adduct including sulfur ligation, ligand oxygenation, and comparisons with all nitrogen ligand analogues, Inorg. Chem. 46 (2007) 6056–6068, https://doi.org/10.1021/ic700541k.
- [27] C.-Y. Su, S. Liao, M. Wanner, J. Fiedler, C. Zhang, B.-S. Kang, W. Kaim, The copper (I)/copper(II) transition in complexes with 8-alkylthioquinoline based multidentate ligands, Dalton Trans. (2003) 189–202, https://doi.org/10.1039/ B208120M.
- [28] B. Bechlars, D.M. D'Alessandro, D.M. Jenkins, A.T. Iavarone, S.D. Glover, C. P. Kubiak, J.R. Long, High-spin ground states via electron delocalization in mixed-valence imidazolate-bridged divanadium complexes, Nature Chem. 2 (5) (2010) 362–368, https://doi.org/10.1038/nchem.585.
- [29] L.D. Wickramasinghe, R. Zhou, R. Zong, P. Vo, K.J. Gagnon, R.P. Thummel, Iron complexes of square planar tetradentate polypyridyl-type ligands as catalysts for water oxidation, J. Am. Chem. Soc. 137 (41) (2015) 13260–13263, https://doi. org/10.1021/jacs.5b08856.
- [30] G.A. McLachlan, G.D. Fallon, R.L. Martin, L. Spiccia, Synthesis, structure and properties of five-coordinate copper(II) complexes of pentadentate ligands with pyridyl pendant arms, Inorg. Chem. 34 (1) (1995) 254–261, https://doi.org/ 10.1021/ic00105a041.
- [31] A.M. Dittler-Klingemann, F.E. Hahn, Trigonal-bipyramidal copper(II) complexes with symmetric and unsymmetric tripodal tetramine ligands, Inorg. Chem. 35 (7) (1996) 1996–1999, https://doi.org/10.1021/ic9506670.
- [32] A.G. Algarra, M.G. Basallote, C.E. Castillo, M.P. Clares, A. Ferrer, E. García-España, J.M. Llinares, M.A. Máñez, C. Soriano, Geometric isomerism in pentacoordinate Cu2+ complexes: equilibrium, kinetic, and density functional theory studies reveal the existence of equilibrium between square pyramidal and trigonal bipyramidal forms for a Tren-derived ligand, Inorg. Chem. 48 (2009) 902–914, https://doi.org/ 10.1021/jc8013078.
- [33] R. Balamurugan, M. Palaniandavar, R. Srinivasa Gopalan, G.U. Kulkarni, Copper (II) complexes of new pentadentate bis(benzimidazolyl)-dithioether ligands: synthesis, structure, spectra and redox properties, Inorganica Chim. Acta 357 (2004) 919–930, https://doi.org/10.1016/j.ica.2003.09.024.
- [34] E.V. Rybak-Akimova, A.Y. Nazarenko, L. Chen, P.W. Krieger, A.M. Herrera, V. V. Tarasov, P.D. Robinson, Synthesis, characterization, redox properties, and representative X-ray structures of four- and five-coordinate copper(II) complexes with polydentate aminopyridine ligands, Inorganica Chim. Acta 324 (1-2) (2001) 1–15, https://doi.org/10.1016/S0020-1693(01)00495-9.
- [35] R. Balamurugan, M. Palaniandavar, H. Stoeckli-Evans, M. Neuburger, Axial versus equatorial coordination of thioether sulfur: Mixed ligand copper(II) complexes of 2-pyridyl-N-(2'-methylthiophenyl)-methyleneimine with bidentate diimine ligands, Inorganica Chim. Acta 359 (2006) 1103–1113, https://doi.org/10.1016/j. ica.2005.09.062
- [36] S.S. Massoud, F.R. Louka, A.F. Tusa, N.E. Bordelon, R.C. Fischer, F.A. Mautner, J. Vančo, J. Hošek, Z. Dvořák, Z. Trávníček, Copper(II) complexes based on tripodal pyridyl amine derivatives as efficient anticancer agents, New J. Chem. 43 (2019) 6186–6196, https://doi.org/10.1039/C9NJ00061E.
- [37] F.A. Mautner, R.C. Fischer, A. Torvisco, M.M. Henary, F.R. Louka, S.S. Massoud, N. M.H. Salem, Five-coordinated geometries from molecular structures to solutions in copper(II) complexes generated from polydentate-N-donor ligands and pseudohalides, Molecules 25 (2020), https://doi.org/10.3390/molecules/25153376
- [38] Z.D. Georgousis, P.C. Christidis, D. Hadjipavlou-Litina, C.A. Bolos, Synthesis, structural characterization and antioxidant/anti-inflammatory activity of pentacoordinated bis(isoselenocyanato) and bis(isothiocyanato) CuII and NiII complexes with Me5dien: Crystal structure of [Cu(Me5dien)(NCSe)2], J. Mol. Struct. 837 (2007) 30–37, https://doi.org/10.1016/j.molstruc.2006.09.026.
- [39] F.A. Mautner, R. Vicente, S.S. Massoud, Structure determination of nitrito- and thiocyanato-copper(II) complexes: X-ray structures of [Cu(Medpt)(ONO)(H2O)] ClO4 (1), [Cu(dien)(ONO)]ClO4 (2) and [Cu2(Medpt)2(μN, S-NCS)2](ClO4)2 (3) (Medpt=3,3'-diamino-N-methyldipropylamine and dien=diethylenetriamine), Polyhedron 25 (2006) 1673–1680, https://doi.org/10.1016/j.poly.2005.11.008.
- [40] C. Gérard, A. Mohamadou, J. Marrot, S. Brandes, A. Tabard, Synthesis and Characterization of Copper Complexes Containing the Tripodal N7 Ligand Tris2-[(pyridin-2-ylmethyl)amino]ethylamine (=N'-(Pyridin-2-ylmethyl)-N, N-bis2-[(pyridin-2-ylmethyl)amino]ethylethane-1,2-diamine): equilibrium, spectroscopic data, and crystal structures of mono- and trinuclear copper(II) complexes, Helvetica Chim. Acta 88 (2005) 2397–2412, https://doi.org/10.1002/ hlca.200590176.
- [41] R.C. Slade, A. a. G. Tomlinson, B.J. Hathaway, D.E. Billing, The electronic properties of trigonal bipyramidal complexes of the copper(II) ion, J. Chem. Soc. A. (1968) 61–63. 10.1039/J19680000061.

- [42] S. Tyagi, B.J. Hathaway, Crystal structure and electronic properties of bis(2,2'-bipyridyl)-cyanocopper(II) nitrate dihydrate: a correlation of the in-plane angular distortion with the splitting of the electronic spectrum, J. Chem. Soc., Dalton Trans. (1983) 199–203, https://doi.org/10.1039/DT9830000199.
- [43] R. Kuroda, S.F. Mason, T. Prosperi, S. Savage, G.E. Tranter, Solid-state absorption and circular-dichroism spectra of five-co-ordinate trigonal copper(II) complexes: anisotropic contributions to the d–d transition probabilities, J. Chem. Soc., Dalton Trans. (1981) 2565–2572, https://doi.org/10.1039/DT9810002565.
- [44] F. Thaler, C.D. Hubbard, F.W. Heinemann, R. van Eldik, S. Schindler, I. Fábián, A. M. Dittler-Klingemann, F.E. Hahn, C. Orvig, Structural, spectroscopic, thermodynamic and kinetic properties of copper(II) complexes with tripodal tetraamines, Inorg. Chem. 37 (16) (1998) 4022–4029, https://doi.org/10.1021/ic971.2951
- [45] F.A. Mautner, C.N. Landry, A.A. Gallo, S.S. Massoud, Molecular structure of mononuclear azido- and dicyanamido-Cu(II) complexes, J. Mol. Struct. 837 (1-3) (2007) 72–78, https://doi.org/10.1016/j.molstruc.2006.10.005.
- [46] S. Khan, A. Al Masum, Md.M. Islam, M.G.B. Drew, A. Bauzá, A. Frontera, S. Chattopadhyay, Observation of r-hole interactions in the solid state structures of three new copper(II) complexes with a tetradentate N4 donor Schiff base: Exploration of their cytotoxicity against MDA-MB 468 cells, Polyhedron 123 (2017) 334–343, https://doi.org/10.1016/j.poly.2016.11.012.
- [47] H. Nagao, N. Komeda, M. Mukaida, M. Suzuki, K. Tanaka, Structural and electrochemical comparison of copper(II) complexes with tripodal ligands, Inorg. Chem. 35 (23) (1996) 6809–6815, https://doi.org/10.1021/ic960303n.
- [48] R.P.F. Kanters, Y. Ru, A.W. Addison, Some high-potential trithioether chelates of copper, Inorganica Chim. Acta 196 (1) (1992) 97–103, https://doi.org/10.1016/ S0020-1693(00)82965-5
- [49] I. Castillo, V.M. Ugalde-Saldívar, L.A.R. Solano, B.N.S. Eguía, E. Zeglio, E. Nordlander, Structural, spectroscopic, and electrochemical properties of tri- and tetradentate N 3 and N 3 S copper complexes with mixed benzimidazole/thioether donors, Dalton Trans. 41 (2012) 9394–9404, https://doi.org/10.1039/ C2DT207564
- [50] T. Ohta, T. Tachiyama, K. Yoshizawa, T. Yamabe, T. Uchida, T. Kitagawa, Synthesis, structure, and H2O2-dependent catalytic functions of disulfide-bridged dicopper(I) and related thioether—copper(I) and thioether—copper(II) complexes, Inorg. Chem. 39 (19) (2000) 4358–4369, https://doi.org/10.1021/ic000018a.
- [51] A.J. Bard, L.R. Faulkner, Electrochemical Methods: Fundamentals and Applications, 2nd ed., Wiley, New York, 2001.
- [52] S.S. Roy, K. Talukdar, J.W. Jurss, Electro- and photochemical reduction of CO2 by molecular manganese catalysts: exploring the positional effect of second-sphere hydrogen-bond donors, ChemSusChem. 14 (2021) 662–670, https://doi.org/ 10.1002/cssc.202001940.
- [53] R.R. Rodrigues, J.M. Lee, N.S. Taylor, H. Cheema, L. Chen, R.C. Fortenberry, J. H. Delcamp, J.W. Jurss, Copper-based redox shuttles supported by preorganized tetradentate ligands for dye-sensitized solar cells, Dalton Trans. 49 (2) (2020) 343–355, https://doi.org/10.1039/C9DT04030G.
- [54] S. Liu, C.R. Lucas, R.C. Hynes, J.-P. Charland, Structure effects in copper coordination compounds of ligands with thioether, aromatic nitrogen, and ether donors, Can. J. Chem. 70 (6) (1992) 1773–1783, https://doi.org/10.1139/v92-
- [55] R. Balamurugan, M. Palaniandavar, R.S. Gopalan, Trigonal planar copper(I) complex: synthesis, structure, and spectra of a redox pair of novel copper(II/I) complexes of tridentate bis(benzimidazol-2'-yl) ligand framework as models for

- electron-transfer copper proteins, Inorg. Chem. 40 (2001) 2246–2255, https://doi.org/10.1021/ic0003372.
- [56] P.V. Robandt, R.R. Schroeder, D.B. Rorabacher, Cyclic voltammetric characterization of rate constants for conformational change in an electron-transfer square scheme involving a copper(II)/(I) macrocyclic tetrathiaether complex, Inorg. Chem. 32 (18) (1993) 3957–3963, https://doi.org/10.1021/ic00070a031.
- [57] N.M. Villeneuve, R.R. Schroeder, L.A. Ochrymowycz, D.B. Rorabacher, Cyclic voltammetric evaluation of rate constants for conformational transitions accompanying electron transfer. Effect of varying structural constraints in copper (II/I) complexes with dicyclohexanediyl-substituted macrocyclic tetrathiaethers, Inorg. Chem. 36 (20) (1997) 4475–4483, https://doi.org/10.1021/ic960866z.
- [58] V. Leandri, Q. Daniel, H. Chen, L. Sun, J.M. Gardner, L. Kloo, Electronic and structural effects of inner sphere coordination of chloride to a homoleptic copper (II) diimine complex, Inorg. Chem. 57 (8) (2018) 4556–4562, https://doi.org/ 10.1021/acs.inorgchem.8b0022510.1021/acs.inorgchem.8b00225.s001.
- [59] J.P. Perdew, K. Burke, M. Ernzerhof, Generalized gradient approximation made simple, Phys. Rev. Lett. 77 (1996) 3865–3868, https://doi.org/10.1103/ PhysRevLett.77.3865.
- [60] J.P. Perdew, K. Burke, M. Ernzerhof, Generalized gradient approximation made simple [Phys. Rev. Lett. 77, 3865 (1996)], Phys. Rev. Lett. 78 (1997) 1396–1396. doi: 10.1103/PhysRevLett.78.1396.
- [61] W.J. Hehre, R. Ditchfield, J.A. Pople, Self—consistent molecular orbital methods. XII. Further extensions of Gaussian—type basis sets for use in molecular orbital studies of organic molecules, J. Chem. Phys. 56 (5) (1972) 2257–2261, https://doi. org/10.1063/1.1677527.
- [62] F. Weigend, R. Ahlrichs, Balanced basis sets of split valence, triple zeta valence and quadruple zeta valence quality for H to Rn: Design and assessment of accuracy, Phys. Chem. Chem. Phys. 7 (2005) 3297–3305, https://doi.org/10.1039/ B508541A
- [63] F. Weigend, Accurate Coulomb-fitting basis sets for H to Rn, Phys. Chem. Chem. Phys. 8 (2006) 1057–1065, https://doi.org/10.1039/B515623H.
- [64] M.J. Frisch, G.W. Trucks, H.B. Schlegel, G.E. Scuseria, M.A. Robb, J.R. Cheeseman, G. Scalmani, V. Barone, B. Mennucci, A. Petersson, H. Nakatsuji, M. Caricato, X. Li, H. P. Hratchian, A. F. Izmaylov, J. Bloino, G. Zheng, J. L. Sonnenberg, M. Hada, M. Ehara, K. Toyota, R. Fukuda, J. Hasegawa, M. Ishida, T. Nakajima, Y. Honda, O. Kitao, H. Nakai, T. Vreven, J. A. Montgomery, Jr., J. E. Peralta, F. Ogliaro, M. Bearpark, J. J. Heyd, E. Brothers, K. N. Kudin, V. N. Staroverov, R. Kobayashi, J. Normand, K. Raghavachari, A. Rendell, J. C. Burant, S. S. Iyengar, J. Tomasi, M. Cossi, N. Rega, J. M. Millam, M. Klene, J. E. Knox, J. B. Cross, V. Bakken, C. Adamo, J. Jaramillo, R. Gomperts, R. E. Stratmann, O. Yazyev, A. J. Austin, R. Cammi, C. Pomelli, J. W. Ochterski, R. L. Martin, K. Morokuma, V. G. Zakrzewski, G. A. Voth, P. Salvador, J. J. Danneberg, S. Dapprich, A. D. Daniels, Ö. Farkas, J. B. Foresman, J. V. Ortiz, J. Cioslowski, D. J. Fox, gaussian 09, Revision d. 01, Gaussian, Gaussian, 9 Revision d. 01, Gaussian,
- [65] K.B. Ørnsø, E.Ö. Jónsson, K.W. Jacobsen, K.S. Thygesen, Importance of the reorganization energy barrier in computational design of porphyrin-based solar cells with cobalt-based redox mediators, J. Phys. Chem. C 119 (23) (2015) 12792–12800, https://doi.org/10.1021/jp512627e.
- [66] L. Mao, T. Moriuchi, H. Sakurai, H. Fujii, T. Hirao, New tridentate cyclometalated platinum(II) and palladium(II) complexes of N,2-diphenyl-8-quinolinamine: syntheses, crystal structures, and photophysical properties, Tetrahedron Lett. 46 (2005) 8419–8422, https://doi.org/10.1016/j.tetlet.2005.09.120.